2016

The influence of resin rich volumes on the mechanical properties of glass fibre reinforced polymer composites

Lewin, G.

Lewin, G. (2016) 'The influence of resin rich volumes on the mechanical properties of glass fibre reinforced polymer composites', The Plymouth Student Scientist, 9(2), p. 123-159.
http://hdl.handle.net/10026.1/14131

The Plymouth Student Scientist
University of Plymouth

*The Plymouth Student Scientist, 2016, **9**, (2), 123-159*

The influence of resin rich volumes on the mechanical properties of glass fibre reinforced polymer composites

Grant Lewin

Project Supervisor: John Summerscales, School of Marine Science and Engineering (Faculty of Science and Engineering) Plymouth University, Drake Circus, Plymouth, PL4 8AA.

Abstract

Glass fibre composite plates were manufactured using several methods to promote increasing levels of fibre volume fraction (V_f), inversely leading to a lower residual resin content and theoretically smaller resin rich volumes (RRV). The aim of this project is to determine the effect of resin rich volumes on the mechanical properties tested and whether they scale with the increase in V_f. Five test plates were manufactured, the first using hand-lamination (HL) with three further plates produced using resin infusion (RI), with infusion occurring under consolidation pressures of 300, 600 and 900mbar. The fifth plate was infused under full vacuum, ~1000mbar consolidation pressure, and then placed into an autoclave (AC) with the total consolidation pressure reaching 5860mbar. Flexural, tensile and inter-laminar shear strength (ILSS) tests were conducted on samples taken from each plate using an Instron 5582 Universal Testing machine with 100kN load cell in accordance to the relevant British Standard for each method. Where possible, further analysis was conducted in order to validate the results based on the theoretical, experimental and simulated methods used. The recorded V_f across the plates increased from 40.77% (HL) to 49.60% (AC), a real term decrease in residual resin content of 14.91%. Optical analysis confirmed that with the increase in V_f the number and size of RRV within each plate decreased. The Elastic modulus, flexural and tensile strengths each showed an increase in property of 365.2MPa, 6.68MPa & 9.11MPa respectively for each 1% increase in V_f across this range. Across the same range in Vf, the ILSS test specimens showed a decrease in strength of 0.373MPa for each 1% increase in V_f. Based on the conducted experiments it can be concluded that there is a strong positive linear relationship between a decrease in RRV and the modulus, flexural and tensile strengths of the plates tested.

Acknowledgements

I would like to offer thanks to John Summerscales and Richard Cullen for sharing their knowledge on composite materials and their help and guidance in manufacturing the composite panels.

I would also like to thank both Terry Richards and Zoltán Gombos, Plymouth University technicians, for their assistance with carrying out the mechanical testing and optical analysis of the specimens.

Nomenclature

Symbol	Property	Unit
AC	Autoclave	-
A_f	Areal weight of fibre	kg/m^2
CoD	Coefficient of determination	-
COSHH	Control of substances hazardous to health	-
CT	Computerised tomography	-
E_C	Young's Modulus of composite	GPa
E_f	Young's Modulus of fibre	GPa
E_F	Flexural Modulus	GPa
E_m	Young's Modulus of resin	GPa
FET	Flow enhancing tows	-
FMD	Fibre-Matrix-Debonding	-
HL	Hand-Laminated	-
ILSS	Inter-laminar shear strength	MPa
NDT	Non-destructive testing	-
OOA	Out Of Autoclave	-
P	Load at failure	N
Pd	First load drop	N
RI	Resin infusion	-
RIFT	Resin infusion under flexible tooling	-
RoM	Rule of mixtures	
RRA	Resin rich areas	-
RRV	Resin rich volumes	-
RTM	Resin transfer moulding	-
S	Span between supports	m
SBV	Surface breaking voids	-
TC	Transverse cracking	-
UD	Uni-directional	-
UTS	Ultimate tensile strength	MPa
VOC	Volatile organic compounds	-
V_f	Fibre volume fraction	%
V_m	Matrix volume fraction	%
V_v	Void volume fraction	%
W_c	Mass of composite	g
W_f	Mass of fibre	g
W_r	Mass of resin	g

m	Gradient of the linear portion of load/deflection graph	N/m
n	Number of layers required	-
t	Thickness	m
t_i	Mean thickness (ILSS)	m
t_f	Mean thickness (Flex)	m
w	Width	m
w/o	Weight percentage	%
η_d	Fibre diameter distribution factor	-
η_l	Fibre length distribution factor	-
η_o	Fibre orientation distribution factor	-
k	Fibre area correction factor	-
ρ_c	Laminate density	kg/m^3
ρ_e	Experimental laminate density	kg/m^3
ρ_f	Fibre density	kg/m^3
ρ_m	Matrix density	kg/m^3
ρ_t	Theoretical laminate density	kg/m^3
σ_C	Strength of composite	MPa
σ_f	Strength of fibre	MPa
σ'_F	Flexural Strength	MPa
σ_m	Strength of matrix	MPa

Contents

List of Figures

List of Tables

1. Introduction

There is a push within the aviation industry to constantly reduce the weight of aircraft. Excess weight means increased costs due to the additional fuel required for take-off. This has led to a greater use of composite materials in aircraft, due to the high strength-to-weight and stiffness-to-weight ratios of the materials (Mraz, 2014).

A standard method of manufacture for aerospace grade components is the use of “prepreg” materials with autoclave consolidation and cure. “Prepreg” is primarily a (carbon) fibre reinforcement that has been pre-impregnated with a thermosetting/thermoplastic resin.

Autoclave use has high acquisition costs, is energy intensive and requires long process times (Witik et al. 2012), therefore the aerospace industry is considering using out-of-autoclave (OOA) processes to reduce costs.

Composite mechanical properties are strongly related to the proportion of fibres to resin, or fibre volume fraction (V_f), since the mechanical properties of fibres are normally much greater than those of resin. Resin usually has much lower stiffness and much higher thermal expansion/contraction in comparison (Dong, 2011).

The compressibility of a fabric determines the maximum achievable V_f (Williams et al. 1998). Moving away from autoclave consolidation, a reduction in applied consolidation pressure will inevitably lead to a small reduction in V_f for a given reinforcement architecture and consequential increase in component weight due to the additional matrix.

This reduction in consolidation pressure can cause resin rich volumes (RRV) within the laminate microstructure due to the remaining residual resin. These volumes are typically referred in literature to as resin-rich-areas (RRA), regions (RRR) or zones (RRZ) due to their quantification through optical analysis. RRV more accurately describes the 3D nature of these features.

For maximum theoretical mechanical properties, the fibres within the laminate should be uniformly distributed with the resin perfectly saturated throughout. In reality, the method of manufacture (Kuriyama et al., 2003. Stickler and Ramulu, 2001. & Mouritz, 2007) and fibre architecture (Basford et al., 1995) will both play a part in disrupting this lack of “perfect” uniform distribution.

1.1. Aims

To ascertain whether mechanical properties of composites scale with fibre volume fraction, or if there is a greater reduction in mechanical properties as the proportion of resin increases.

1.2. Objectives

- Manufacture laminates using a single batch of 270 gm^{-2} biaxial plain-weave glass fibre reinforcement in combination with an unsaturated polyester resin using:
  - Minimal pressure through hand lay-up.
  - 300 mbar positive pressure using RI. (≈ 700 abs.)
  - 600 mbar positive pressure using RI. (≈ 400 abs.)
  - 900 mbar positive pressure using RI. (≈ 100 abs.)
  - RI (≈1000mbar) plus circa 5000 mbar positive pressure in the autoclave.
- Determine the fibre volume fraction (V_f), void volume fraction (V_v) and resin volume fraction (V_m) for each test panel.
- Conduct mechanical testing on samples taken from each of the plates based on the following standards:
  - Tensile (strength & modulus) testing - BS EN ISO 527 – 4.
  - Flexural (strength & modulus) testing - BS EN ISO 14125:1998+A1:2011.
  - Inter-laminar shear strength testing - BS EN ISO 14130:1998.
- Where possible, validation of results will be sought through alternative methods.
- Compare the calculated value for V_f against the mechanical properties to determine if there is a correlation and whether the properties scale.

2. Literature review (*)

2.1. Fibre volume fraction (V_f)

There are a multitude of processes available for the manufacture of composites (Åström, 1997, & Daniel and Ishai, 2006). The method used can depend on a variety of factors such as; number of components, cost, mechanical properties required and the desired shape. Each method inherently has its advantages and disadvantages in comparison to the others, with the selected method governing the quality of the laminate produced.

The maximum achievable V_f is determined through the method of manufacture and is a function of the applied consolidation pressure as well as the compressibility of the fabric. Research conducted by Quinn and Randall (1990) proposed the value of V_f is a function of the square root of pressure, with an alternate theory proposed by Toll (1998) who concluded the pressure vs V_f power law exponents were higher than 2.

Robitaille and Gauvin (2004) conducted a review of published experimental data and observed that V_f increased rapidly with pressure on the fibre stack. As the laminate approaches the maximum possible V_f, there is minimal change for the increased pressure up to a maximum value of 1000mbar. This is expected, as once the fibre has reached its maximum compressibility there is no room for an increased V_f regardless of additional pressure applied.

Williams et al. (1998) produced laminate panels using resin infusion under flexible tooling (RIFT) and concluded the resin appears to lubricate the fibres/fabric under the influence of a vacuum and can result in a further reduction in thickness/increase in V_f.

Consolidation pressure can range from zero for hand-lamination, a maximum of ≈1000mbar for resin infusion, to a typical working pressure of 5000-7000mbar (Pickard, n.d.) in an autoclave. Comparing these methods based on an identical fabric and number of layers, the V_f will differ due to the volume of residual resin (V_m) in each panel whereby $V_m=1-V_f$ (assuming $V_v=0$). Unless the fibres are uniformly distributed within the laminate, the residual resin will inherently lead to RRV's in both the inter-tow and inter-ply regions.

2.2. Location of resin rich volumes (RRV)

The location and size of RRV have been found to be affected by both the method of construction and the fabric architecture. Basford et al. (1995) manufactured laminate panels using the Resin Transfer Method (RTM) method from twill-weave carbon fibre that included 'flow enhancing' tows (FET) distributed throughout the fabric. The additional (FET) lead to large RRV forming adjacent to these within the fabric architecture.

This leads to the suggestion that the volumes seen between the fibre tows in a woven fabric provide a natural space for resin to remain, regardless of how well the layers/fibres compress together and consolidation pressure applied.

Aono et al. (2008) conducted fatigue testing on both unidirectional (UD) and double bias mat (DBM) laminates and concluded the fatigue damage initiated from RRV, stitches and 90^0 strands. Stickler and Ramulu (2001) tested transverse stitched T-joints in both flexure and tension. Results showed that flexural specimens failed in part due to high stress concentrations seen in the "resin rich" fillet region. In z-pinned composite panels produced by Mouritz (2007), RRV were identified in the area surrounding the location of the z-pin as it passed through the reinforcement material.

2.3. Voids

Defects within a composite are primarily found in the matrix, therefore the presence of RRV within a composite provides the space in which these can occur. The two most prevalent fabrication defects within solid laminates are porosity and foreign objects (Campbell, 2010). Porosity, in the form of voids, can be introduced in various ways depending on the method of manufacture.

Judd and Wright (1978) summarised the wide variety of void classifications into two distinct categories; voids along individual filaments and voids between laminae. For laminates manufactured using a liquid resin matrix, a cause of void introduction is air bubbles. These can become trapped in the resin (Figure 3) during its preparation or within the laminate as the resin moves through the fabric, regardless of the process used. De-gassing is a method that can help eliminate voids before resin use.

Another cause for bubbles within the matrix is volatile organic compounds (VOC). These may be essential components of the resin, such as styrene in UPE, or form due to the chemical reaction that takes place.

The void volume fraction (V_V) is an important quality characteristic within a composite. Ghiorse (1993) discussed that for high quality composite applications, such as those used in aerospace structures, void content levels above 1% are unacceptable. For less critical applications, a V_V of up to 5% may be acceptable.

Judd and Wright (1978) investigated voids and their influence on the mechanical properties of composites. For inter-laminar shear stress, a matrix dominated property, they reported there was a 7% decrease in shear strength for each 1% increase in void content up to a total void content of 4%.

Summerscales (no date. A) summarised the work of Stone and Clarke (1975), who reported that below V_v= 1.5% voids tend to be volatile-induced and hence spherical with diameters in the range 5-20μm. Above V_v= 1.5%, the voids are flattened and elongated in the in-plane direction due to the limitation of space between the fibre bundles and are also significantly larger than those voids at a lower V_v.

The negative effects of voids have been investigated in relation to other mechanical properties of composites. Liu et al. (2006) conducted three-point flexural, tensile and ILSS tests on $[0/90]_{3S}$ laminates manufactured with varying void contents. Results showed a decrease in tensile strength of 14% for an increase in void content from 0.6 to 3.2%. In flexure, a 22% decrease in flexural strength was recorded for a void content of 3.2%.

A reduction in tensile strength was also witnessed by Zhu et al. (2008) who investigated the effect of voids on the tensile properties of $[(\pm45)_4/(0/90)/(\pm45)_2]_S$ and $[(\pm45)/_4/(\pm45)(0/90)]_S$ composites produced in an autoclave. It was observed that as V_V increased, so too did the size and aspect ratio of the voids. A reduction in tensile strength was recorded for both stacking sequences, with both also displaying signs that cracks initiated from the voids.

2.4. Identification and measurement of V_F, RRV and Voids

A density check is a method for assessing void content, with the water displacement method based on the Archimedes' principle. This entails measuring the weight of the laminate both in air and in water (Liu et al. 2006). The V_v is then calculated based on the theoretical density of the laminate with no voids present. In order to accurately determine this, the density of the fibres and cured resin must be known.

Matrix combustion in a muffle furnace, a destructive method whereby the matrix is physically removed by ignition was used by Valenza and Fiore (2010) to establish the values for fibre, matrix and void content according to the standard ASTM 3171.

Non-destructive testing (NDT) methods allow the inspection of components (Summerscales, (1987) & Summerscales, (1990b)) to determine their structural integrity/quality both prior to further use, or following failure, without causing further damage to the component.

Summerscales (1990a) conducted a review of advances in NDT methods and summarised the techniques under three headings; electromagnetic, spectroscopic and mechanical. From the range of processes available the methods predominantly used for analysis of V_f, RRV's and voids are radiography (X-ray), computerised tomography (CT) and optical microscopy with image analysis (Guild and Summerscales, (1993) and Summerscales, (1998)). The benefit of each is their ability to generate an image of the internal structure of the laminate

Tan et al. (2013) used transmission radiography, in combination with ultrasonic C-scan and X-ray micro-computed tomography to study fractured samples, and found damage initiation occurs at a lower load in stitched composites due to RRV which act as crack initiation sites.

Carbon-fibre/epoxy plates, manufactured using resin transfer moulding (RTM), were inspected by Pearce et al. (2000) using optical microscopy and imaging analysis. Multiple images were taken of the microstructure under a microscope, with these stitched together to form a continuous representation of the sample which was then analysed to determine the fractal dimension for each of the four fabrics used.

3. Methodology

3.1. Constituent Materials

3.1.1. Fabric and lay-up

The fabric was a 270 g/m^2 plain woven biaxial glass fibre. Analysis of a 100mm^2 sample confirmed the stated areal weight (A_f) and that the fabric was unbalanced (a balanced fabric would have an equal number of tows in both warp and weft directions) see Figures 4a&b.

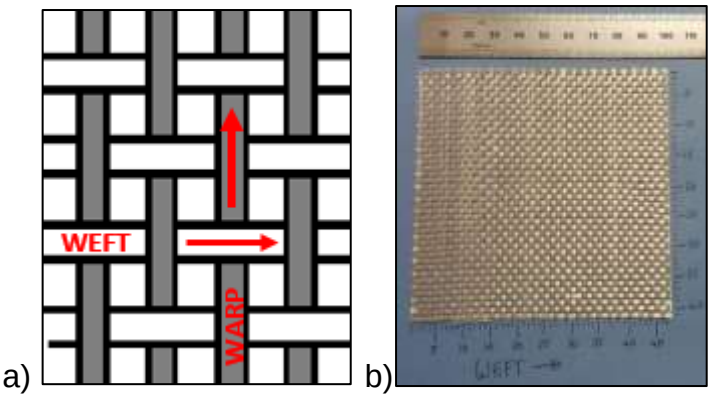

Figure 1: Fabric characterisation. a) Warp and weft directions. b) Analysis of fabric used throughout.

The number and weight of tows in each direction (Table 1) were determined through separating and counting/weighing each. Nine plies were used to create the 2mm thick panels required by the test standards.

Table 1: Comparison of fibre warp and weft directions.

Direction.	No. of tows.	Total weight of tows.	Individual weight.
Warp	47	1.26g	268 mg/tow
Weft	41	1.44g	351 mg/tow

A $0^o/90^o$ ply orientation was maintained throughout, ensuring both warp and weft plies each remained parallel throughout the laminate due to the unbalanced nature of the fabric and the effect this might have on the comparative properties.

3.1.2. Resin system.

Easy Composites IP2 polyester infusion resin and 2% w/o Butanox M50 MEKP catalyst were used throughout, with consideration given to the relevant COSHH sheets. Prior to use, the resin was warmed to 25^oC to ensure constant viscosity independent of the ambient conditions on the day.

3.2. Laminate panel manufacture

Early in the project, the use of out-dated resin lead to the scrapping of the first 5 manufactured panels. There are a significant number of other variables that can influence the outcome and overall quality of a laminate, with some highlighted in Table 2.

Table 2: Possible variables that may influence manufactured laminates.

Variable		
Temperature	Time of day	Stacking sequence
Relative humidity	Resin viscosity	Vacuum achieved
Pressure	Mixing of resin	Leak rate
Consumables	Duration under vacuum	Post-cure

To minimise and monitor any variability between panels, an experimental data record sheet was completed for each experiment.

To achieve the desired variation in V_f, the panels were manufactured using increasing consolidation pressure, with a constant number of plies throughout. The base-line was a hand-laminated panel, with a “consolidation” roller used to wet out the fibres, with the consolidation pressure deemed negligible relative to the pressures applied to the remaining panels.

All other panels were manufactured using (RIFT) with a flow mesh to aid resin flow. For the purpose of this project, consolidation pressures of 300, 600 & 900mbar were selected for the infusions. The final panel was infused at full vacuum and then immediately placed into an Autoclave whereby a total consolidation pressure of 5860mbar was applied.

To prevent over consolidation, due to the non-elastic response of the fabric, at no point during the manufacture of the panels (including leak rate checks)

were the fibres exposed to a consolidation pressure greater than that of the experiment, as this would result in a false reading for V_f.

3.2.1. Hand-laminated panel.

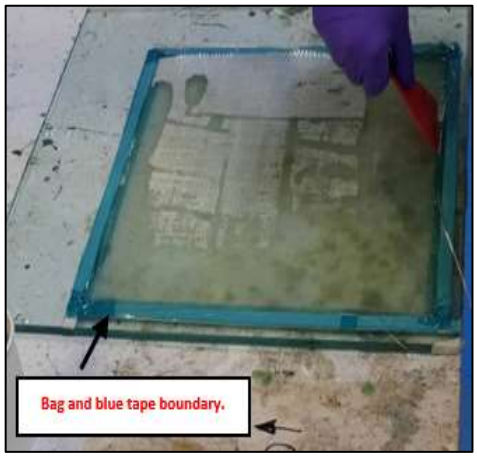

Figure 2: Hand-laminated panel manufacture.

To ensure results were comparable, IP2 RI resin was used as the matrix for the hand-laminated panel. To prevent run off due to the low resin viscosity, a cavity of 355mm^2 was framed on a glass mould plate using two layers of bag tape covered in “blue tape” (Figure 2). This created a barrier to prevent resin loss with the lay-up arrangement. Table 3 shows the ambient conditions at the time of manufacture.

Table 3: Hand-laminated panel ambient conditions.

Experiment.	Time.	Temp. (°C)	Relative Humidity	Pressure. (mbar Abs.)
HL	1500	18	34%	1007 ± 2

3.2.2. Resin infused panel manufacture.

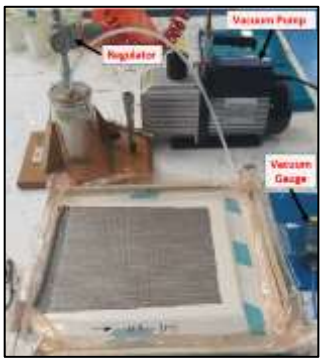

Figure 3: Variable infusion pressure set-up.

The RI panels were manufactured using a process that involved a pressure regulator on the outlet providing a means of controlling the pressure applied (Figure 3).

Before applying the vacuum, the ambient pressure was recorded and target pressure determined. Once applied, the pressure was increased to the required level using the vacuum gauge as reference, ensuring no more than required (±5 mbar) was applied. Table 4 shows the experimental values recorded on the application of the vacuum. Each panel remained under vacuum for 2 hours prior to infusion.

Table 4: Experimental data recorded for the three RI test panels.

Experiment.	Time.	Temp. (^{o}C)	Relative Humidity	Pressure. (mbar Abs.)	Target pressure. (mbar Abs.)	Pressure achieved. (mbar Abs.)	Vacuum loss. (mbar/min)
300	0900	16	59%	1010 ± 2	710	711 ± 2	0.1 ± 2
600	0900	15	41%	1004 ± 2	404	404 ± 2	0 ± 2
900	0900	15	37%	990 ± 2	90	90 ± 2	0 ± 2

3.2.3. Autoclave panel manufacture.

Figure 4: Autoclave test panel lay-up.

The autoclave panel was laid up (Figure 4) and infused under full vacuum, as per a standard infusion method. The mould plate for the experiment was 600mm x 600mm, with a 550mm x 500mm layer of peel ply used as a “resin trap” for any excess resin removed from the panel under consolidation in the autoclave.

Once the resin was identified as having fully wetted out the fibres, both inlet and outlet pipes were clamped with the entire panel placed into an Aeroform autoclave and the total pressure on the laminate raised to and maintained at 5860±150 mbar for a duration of 5 hours. The temperature recorded throughout was 35±2^{o}C, the minimum achievable during autoclave operation. Table 5 shows the experimental values recorded on the application of the vacuum.

Table 5: Ambient conditions on application of vacuum for the autoclave panel.

Experiment.	Time.	Temp. (^{o}C)	Relative Humidity	Pressure. (mbar Abs.)	Pressure Achieved. (mbar Abs.)	Vacuum loss. (mbar/min)
AC	1100	17	44%	1010 ± 2	8.5 ± 2	0.1 ± 2

An alternative method using bleeder cloth as the “resin trap” was initially used, however this proved unsuccessful due to not balancing the volume of space provided with the level of resin removed, with capillary flow drawing the resin from the panel.

3.3. Validation

Several methods were used in an attempt to further validate the results from both experiments and calculations.

3.3.1. Resin burn-off

To validate the V_f calculated using Equation 1, resin burn-off was conducted. This method is based on CRAG method 800 which entailed weighing samples using an Avery-Berkel Analytical Balance (last calibrated 10/06/2004) in both air and water before placing the samples in a furnace. Once all the resin was burnt off, the bare fibres were then reweighed.

3.3.2. Simulation

Autodesk Simulation Composite Design 2014 software was used to simulate the manufactured panels. Inputting both measured values and assumptions made for the constituent material properties, the software is capable of predicting values such as the Elastic Modulus. These simulated values were then used for comparison against those determined theoretically and experimentally.

3.3.3. Rule of Mixtures

Equation 1 shows the R-o-M equation (Virk et.al. 2012) used to calculate the theoretical modulus of elasticity for each of the panels.

$E_C = (\kappa^* \eta_d^* \eta_l^* \eta_o^* V_f^* E_f) + (V_m^* E_m)$	Where: $\mathbf{E_C}$ = Modulus of the composite $\boldsymbol{\kappa}$ = Fibre area correction factor (set as unity) $\boldsymbol{\eta_d}$ = Fibre distribution factor (set as unity) $\boldsymbol{\eta l}$ = Fibre length distribution factor $\boldsymbol{\eta_o}$ = Fibre orientation distribution factor $\mathbf{V_f}$ = Fibre volume fraction $\mathbf{E_f}$ = Modulus of the fibres $\mathbf{V_m}$ = Matrix volume fraction $\mathbf{E_m}$ = Modulus of the matrix	<1>

Equation 1: Rule of Mixtures.

The fibre orientation distribution factor was had to be calculated due to the unbalanced nature of the fabric.

3.3.4. Kelly – Tyson strength model

Equation 2 shows the Kelly – Tyson model (1965) for UD composites, used to predict the ultimate tensile strength (UTS) for each panel to compare against the experimental results.

$\sigma_C = (\sigma_f * V_f) + (\sigma_{m^*} * (1 - V_f)$	Where: σ_C = Predicted ultimate tensile strength of composite. σ_f = ultimate tensile strength of the fibre. V_f = Fibre volume fraction. σ_{m^*} = tensile stress in the matrix at the failure strain of the fibre.	<2>

Equation 2: Kelly - Tyson model for ultimate tensile strength with transverse fibres omitted from analysis.

3.4. Mechanical testing

Specimens were cut from specific areas of the plate, with an identification number and their orientation based on the plate marked on each. Each standard recommends taking specimens from locations across the plate, however in order to recoup lost time during manufacture a decision was made to take the samples as a block, with an identical location used for each experiment.

The specimens were cut using a Tyslide diamond wheel slitting saw to dimensions according to the standard related to each test method. All specimens were measured to ensure conformity with the parameters stated in the relevant standard. The number of measurements taken for both thickness and width of each specimen type, using a micrometer capable of measuring to ±0.01mm, are shown in Table 6.

Table 6: Number of specimen measurements recorded.

Test specimen.	No. of measurements.	Distance between measurements.
ILSS	3	4 mm
Flexural	5	10 mm
Tensile	7	35 mm

Testing was conducted on an Instron 5582 with 100kN load cell with Table 7 showing the parameters for each test method.

Table 7: Mechanical test information.

Test method.	Test standard.	Span.	Cross-head speed.	Last calibrated.
Flexural.	BS EN ISO 14125:1998+A1:2011.	1. 40 mm 2. 48mm	1 mm/min	June 2007
ILSS	BS EN ISO 14130:1998	1. 10 mm 2. 11.4 mm	1 mm/min	June 2007
Tensile	BS EN ISO 527 – 4	-	2mm/min	June 2007

3.5. Analysis

3.5.1. Surface analysis

Surface analysis was conducted on a 100mm^2 area in the centre of each panel to quantify a value for surface breaking voids (SBV). Carbon dust was applied to the mould face surface to fill any SBV, with an image captured of each.

After converting the images to binary, with individual pixels either 'on' (black) or 'off' (white), ImageJ software was used to determine the percentage area of remaining 'on' pixels from the total image area.

3.5.2. Optical analysis

25mm long warp and weft samples from an identical location in each panel were potted in epoxy and polished using a Buehler Automet 250 grinder/polisher (Figure 5b).

a)  b) 

Figure 5: a) Olympus SC50 Optical Microscope. b) Buehler Automet 250 grinder polisher.

Three images of each specimen were analysed using an Olympus SC50 optical microscope (Figure 5a) and Olympus Stream software to assess the size and location of any RRV (as areas) within the laminates. Optical analysis was also used to confirm the failure mode for each specimen.

3.5.3. Void volume fraction

Equation 3 (Judd and Wright, 1978) was used in an effort to determine the V_v of the laminate panels.

$V_v = \frac{W_c}{\rho_c} - \left(\frac{W_f}{\rho_f} + \frac{W_r}{\rho_r}\right)$	Where: V = volume fraction W = weight ρ = density	Subscripts: v = voids c = composite f = fibre r = resin	<3>

Equation 3: Void volume fraction calculation.

4. Results

4.1. Surface analysis

Table 8 shows the percentage SBV's based on the image for each panel.

Table 8: Percentage surface breaking voids.

Experiment No.	**HL**	**300**	**600**	**900**	**AC**
Surface breaking voids (%)	1.93	2.42	1.43	0.31	0.02

4.2. Panel thickness

Table 9 shows the plate thicknesses recorded.

Table 9: Mean panel thickness based on the measurement of test specimens.

		Experiment				
Property	**Unit**	**HL**	**300**	**600**	**900**	**AC**
TENSILE SPECIMENS						
Mean specimen thickness	mm	2.33	2.08	2.03	1.94	1.92
Standard deviation	-	0.049	0.025	0.041	0.011	0.016
Coefficient of variation	%	2.082	1.217	2.004	0.577	0.857
FLEXURAL SPECIMENS						
Mean specimen thickness	mm	2.39	2.09	2.07	1.95	1.94
Standard deviation	-	0.025	0.009	0.026	0.013	0.005
Coefficient of variation	%	1.033	0.437	1.246	0.668	0.257
INTER-LAMINAR SHEAR SPECIMENS						
Mean specimen thickness	mm	2.32	2.11	2.00	1.93	1.92
Standard deviation	-	0.012	0.025	0.017	0.008	0.012
Coefficient of variation	%	0.510	1.183	0.849	0.431	0.612
OVERALL PLATE						
Plate thickness (mean)	**mm**	**2.34**	**2.09**	**2.03**	**1.94**	**1.93**
Standard deviation	**-**	**0.058**	**0.037**	**0.050**	**0.023**	**0.026**
Coefficient of variation	**%**	**2.492**	**1.756**	**2.454**	**1.199**	**1.329**

4.3. Fibre volume fraction

Table 10 shows each panel fibre volume fraction based on the mean value of test specimens as well as that determined using the resin burn off method.

Table 10: Fibre volume fraction determined through both calculation and resin burn-off.

		Experiment				
Property	**Unit**	**HL**	**300**	**600**	**900**	**AC**
Tensile specimen V_f (mean)	%	40.98	46.08	47.04	49.25	49.87
Flexural specimen V_f (mean)	%	40.02	45.75	46.15	49.18	49.20
ILSS specimen V_f (mean)	%	41.32	45.30	47.90	49.56	49.72
Plate V_f (mean) (using values above)	**%**	**40.77**	**45.71**	**47.03**	**49.33**	**49.60**
Standard deviation	-	0.438	0.243	0.667	0.185	0.580
Coefficient of variation	%	1.074	0.531	1.418	0.376	1.169
Burn-off panel V_f	**%**	**41.99**	**46.54**	**46.72**	**48.12**	**50.86**

4.4. Void volume fraction

Table 11 shows the void volume fraction calculated using equation <3>.

Table 11: Void volume fractions determined based on the densities of the constituent materials.

		Experiment				
Property	**Unit**	**HL**	**300**	**600**	**900**	**AC**
E-glass density of 2550 kg/m^3						
Void volume fraction (Eq. 3)	%	-1.73	-0.18	-0.97	-1.16	-1.15
E-glass density of 2600 kg/m^3						
Void volume fraction (Eq. 3)	%	-0.74	0.91	0.14	-0.03	0.05

4.5. Elastic modulus

Table 12 shows the elastic modulus determined for each of the panels.

Table 12: Elastic modulus determined based on different methods.

		Experiment				
Property	**Unit**	**HL**	**300**	**600**	**900**	**AC**
Rule of Mixtures	GPa	17.879	19.611	20.072	20.883	20.975
Laminate Analysis	GPa	19.025	21.200	21.765	22.830	22.860
Experimental (Flexural)	GPa	18.690	19.752	19.775	21.115	22.349
Experimental (Tensile)	GPa	21.906	23.740	24.514	24.926	25.031

4.6. Flexural Strength

Table 13 shows the initial and flexural strength determined for each of the panels.

Table 13: Calculated flexural strength of the panels.

		Experiment				
Property	**Unit**	**HL**	**300**	**600**	**900**	**AC**
INITIAL FLEXURAL STRENGTH @ 40mm SPAN						
Mean initial flexural strength	**MPa**	240.904	277.387	237.556	237.965	235.339
Standard deviation	-	9.393	21.960	15.759	7.441	4.828
Coefficient of variation	%	3.899	7.917	6.634	3.127	2.052
INITIAL FLEXURAL STRENGTH @ 48mm SPAN						
Mean initial flexural strength	**MPa**	229.067	243.570	227.428	248.563	253.296
Standard deviation	-	12.503	20.706	28.089	17.019	6.747
Coefficient of variation	%	5.458	8.501	12.351	6.847	2.664
FLEXURAL STRENGTH @ 40mm SPAN						
Mean flexural strength	**MPa**	578.443	611.796	614.238	641.089	690.934
Standard deviation	-	14.031	6.430	12.238	26.692	23.933
Coefficient of variation	%	2.426	1.051	1.992	4.164	3.464
FLEXURAL STRENGTH @ 48mm SPAN						
Mean flexural strength	**MPa**	558.734	578.373	586.315	599.838	608.133
Standard deviation	-	7.192	12.972	11.047	20.871	12.896
Coefficient of variation	%	1.287	2.243	1.884	3.479	2.121

4.7. Inter-laminar Shear

Table 14 shows the initial and ILSS determined for each of the panels.

Table 14: Inter-laminar shear properties.

		Experiment				
Property	**Unit**	**HL**	**300**	**600**	**900**	**AC**
INITIAL INTER-LAMINAR SHEAR STRENGTH@ 10mm SPAN						
Mean initial shear strength	**MPa**	**46.108**	**43.585**	**43.176**	**43.838**	**43.604**
Standard deviation	-	0.593	2.036	1.170	2.247	0.892
Coefficient of variation	%	1.286	4.672	2.711	5.125	2.046
INITIAL INTER-LAMINAR SHEAR STRENGTH @ 11.4mm SPAN						
Mean initial shear strength	**MPa**	**42.945**	**40.142**	**42.267**	**40.486**	**40.711**
Standard deviation	-	1.452	2.603	1.003	0.937	1.311
Coefficient of variation	%	16.244	6.484	2.374	2.315	3.220
INTER-LAMINAR SHEAR STRENGTH @ 10mm SPAN						
Mean inter-laminar shear strength	**MPa**	**56.429**	**53.504**	**54.059**	**53.361**	**52.537**
Standard deviation	-	0.842	1.312	1.428	1.557	1.052
Coefficient of variation	%	1.492	2.452	2.642	2.918	2.002
INTER-LAMINAR SHEAR STRENGTH @ 11.4mm SPAN						

Mean inter-laminar shear stress	**MPa**	**52.458**	**49.899**	**51.165**	**46.641**	**48.648**
Standard deviation	-	1.675	1.677	0.592	0.937	1.025
Coefficient of variation	%	3.193	3.361	1.158	2.009	2.106

4.8. Tensile properties

Table 15 shows the apparent tensile fibre-matrix-debonding (FMD) strain & load as well as modulus and strength properties determined for each of the panels.

Table 15: Values determined through both experimental testing and prediction for tensile properties of the manufactured panels.

		Experiment				
Property	**Unit**	**HL**	**300**	**600**	**900**	**AC**
APPARENT FMD/ TRANSVERSE CRACKING STRAIN						
Mean panel FMD strain	**%**	0.213	0.223	0.247	0.257	0.263
Standard deviation	-	0.029	0.034	0.017	0.019	0.021
Coefficient of variation	%	13.441	15.221	6.891	7.347	7.803
APPARENT FMD/ TRANSVERSE CRACKING LOAD						
Mean panel FMD load	**kN**	**2.563**	**2.622**	**2.763**	**2.965**	**3.203**
Standard deviation	-	0.087	0.035	0.034	0.132	0.160
Coefficient of variation	%	3.404	1.319	1.249	4.438	5.005
TENSILE MODULUS						
Mean panel modulus	**GPa**	**21.906**	**23.740**	**24.514**	**24.926**	**25.031**
Standard deviation	-	0.582	0.331	0.562	0.433	0.186
Coefficient of variation	%	2.657	1.392	2.291	1.737	0.744
TENSILE STRENGTH						
Mean panel strength	**MPa**	**383.584**	**466.083**	**425.636**	**452.275**	**477.947**
Standard deviation	-	14.647	19.617	26.022	31.026	24.381
Coefficient of variation	%	3.819	4.209	6.114	6.860	5.101
KELLY – TYSON PREDICTED STRENGTH						
Predicted strength	**MPa**	**489.295**	**541.975**	**551.891**	**574.719**	**581.123**
DIFFERENCE						
Predicted – Experimental	MPa	105.7	75.9	126.3	122.4	103.2
Percentage Difference	%	21.60	14.00	22.88	21.30	17.75

Note: Percentage difference = (1 – (Experimental/Predicted))*100

5. Discussion

5.1. Causes of variation in results

Variation between results could be accounted for in the methods used; those being theoretical calculations based on empirical data, computer generated simulation or experimental testing. Underlying assumptions, simplifications or

errors in each method could affect the resultant value. Table 16 highlights some possible causes of variation for each method.

Table 16: Possible causes of variation between the different methods used to determine results.

Method	Assumptions/possible cause of variation.
RoM	**Assumes:** ➢ Fibres are uniform, parallel and continuous. ➢ Perfect bonding has occurred between fibre and matrix. ➢ There is constant thickness, therefore V_f, throughout.
Laminate analysis	**Assumes:** ➢ Fibres are perfectly distributed and concentrated towards neutral axis of layer. ➢ Zero V_v. ➢ The software is reliant on accurate knowledge of material properties.
Experimental	➢ Imperfections during manufacture, such as voids/fibre misalignment. ➢ Specimen location on panel. ➢ Incorrect test method/interpretation of results. ➢ Use of equipment with out-dated calibration certificates.

5.2. Determining the statistical correlation of the data

To ascertain the significance of the data to a given trend, the coefficient of determination (CoD), or R^2 value will be used to describe how closely the data conforms to a linear relationship.

An R^2 value ranges from 0-1, with a value of 1 indicating a perfect match between data and regression line, whilst a value of 0 signals there is no relationship between the data points. An R^2 value of 0.5 shows that 50% of the variance in (*y)* is predictable from a value from (*x)*.

5.3. Constituent Volume Fractions

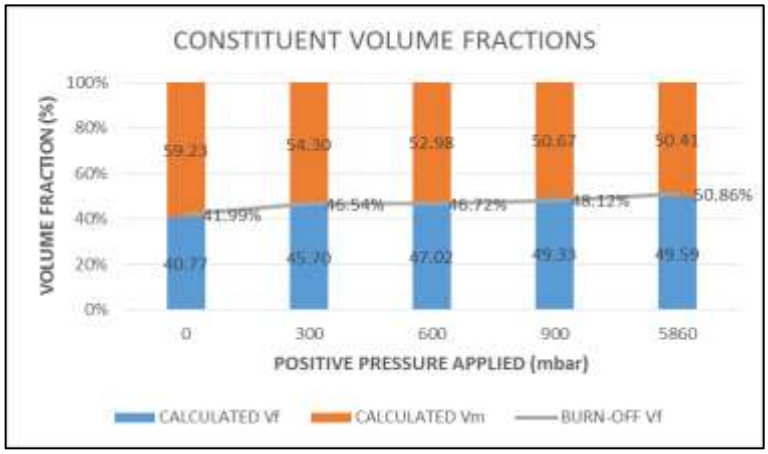

Figure 6: Comparison of fibre volume fractions

Figure 6 shows that as the applied pressure increases there is an increase in V_f as expected. The OOA panels V_f increases by +8.56% between applied pressures of zero and 900 mbar.

For the AC panel there is a further increase in pressure of 551%, but only a 0.26% increase in fibre content. This reduced rate of increase in V_f relates to the maximum compressibility of a fabric (Quinn & Randall (1990) and Toll & Månson (1994)), suggesting that at 900mbar the fabric is already close to its maximum value, as reported by Robitaille and Gauvin (2004). The additional consolidation pressure reduces the volume between fibres, preventing the flow path of resin, hence the insignificant reduction in V_f between the two.

Figure 6 shows there is little difference in V_f, with a maximum deviation of 2.9%, when comparing the results from calculation and resin burn-off. This confirms the calculated V_f, as lying within acceptable bounds based on the accumulation of possible errors inherent in both methods. Despite spending considerable time attempting to acquire images to further confirm V_f, the low contrast between the glass and the matrix made it impossible to distinguish between the two phases and consistently detect features using the associated software.

5.4. Resin rich volumes

Figures 7a-e show representative through-thickness images of samples taken from each plate, as described in Section 3.6.2. RRA measuring greater than 50000μm2 were manually highlighted using Olympus Stream software, with the resultant measurement “burnt” into the image. Time constraints mean the collected data may not be statistically valid due to the representative area analysed being significantly smaller than the panel.

To quantify the resin as a “volume”, a 3-D image would be required in order to perceive depth, however a representation greater than a 2-D image was not possible with the equipment available.

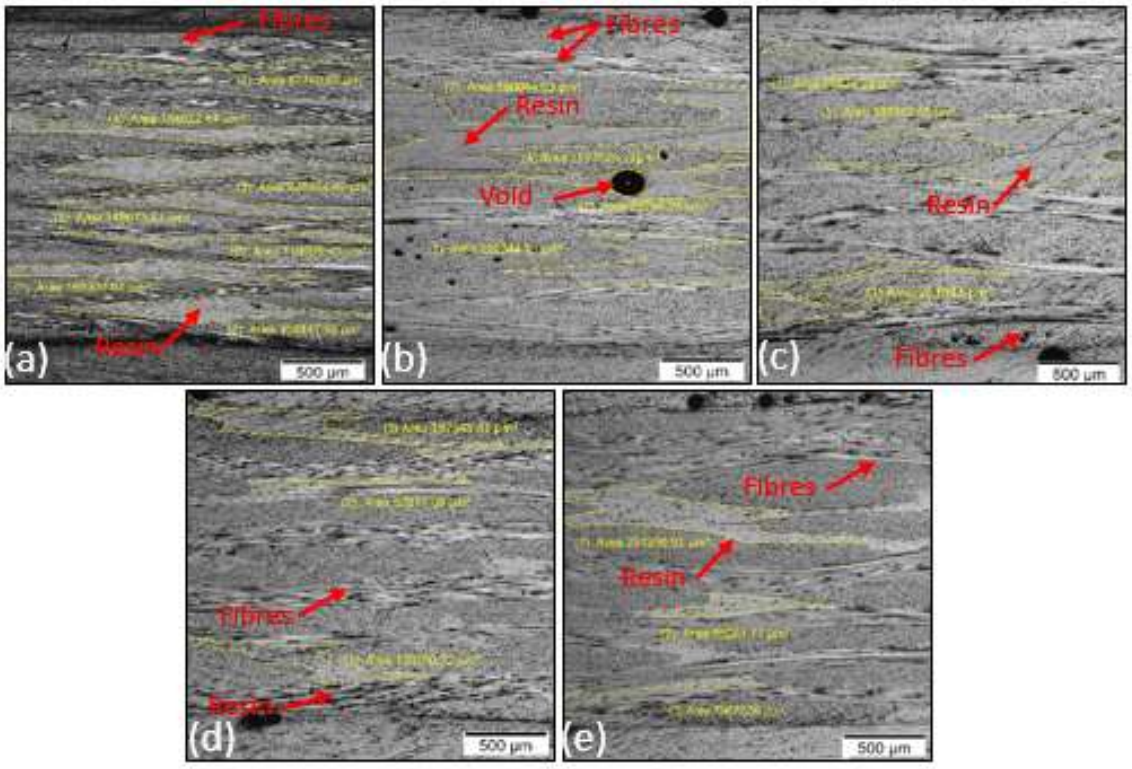

Figure 7. Optical images showing size and number of resin rich areas in through-thickness samples taken from each panel. (a) Hand-laminated (b) 300 mbar (c) 600 mbar (d) 900 mbar (e) Autoclave

Table 17 shows that as V_f increases through the range of consolidation pressures, there is a reduction in the total resin area between the inter-tow and inter-ply regions. Figures 10a-e show that RRV are located in the space between tows where waviness has occurred, with these volumes highlighted as areas of weakness in literature (Aono et al. (2008) and Kuriyama et al. (2003) and Stickler & Ramulu (2001)).

Table 17: Results of measured RRA using optical microscopy on through-thickness samples from the different panels.

		Experiment				
Property	**Unit**	**HL**	**300**	**600**	**900**	**AC**
No. RRA's	-	**7**	**3**	**3**	**3**	**3**
Smallest area	μm^2	67740	115752	68836	52877	65831
Largest area	μm^2	226924	586044	396375	197341	251996
Total area	**μm^2**	**1076057**	**929840**	**666559**	**370409**	**396750**

5.5. Void volume fraction (V_v) and Voids

Due to technical issues the use of automated software to stitch together a large number of individual images taken of through-thickness samples was not available, therefore the analysis undertaken was limited.

A crude alternative was to capture planar images of the surface. Although not a quantitative measure of the through-thickness void presence and location, analysis would provide a representation of the number and size of voids seen. Through manually highlighting any voids visible, ImageJ software could be used to quantify the percentage area occupied by these.

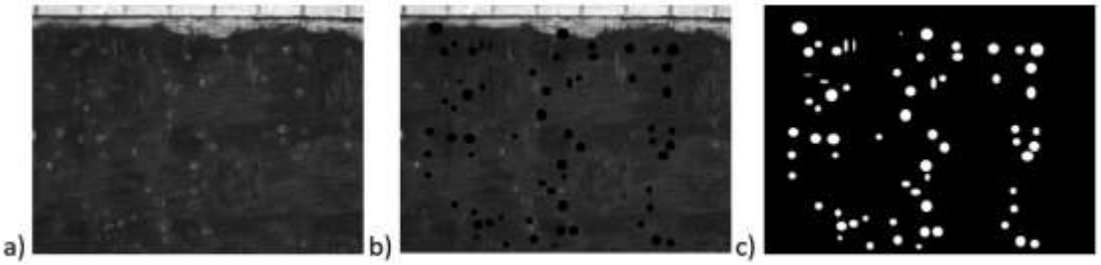

Figure 8: Method for quantifying voids present within each panel. a) Optical image captured under the microscope. b) Edited image having manually identified and highlight potential voids. c) Converted binary image analysed using ImageJ software to quantify the percentage area of the voids.

Figure 8 a-c show the steps taken to process each image with the results for the samples inspected shown in Figure 9. Table 18 shows the 600mbar panel has the highest percentage area of voids. They are fewer in total yet they have a greater average size than the 300mbar panel.

Further investigation is required to determine the reason behind the difference, as an increase in V_f should reduce the volume in which the voids can remain. An explanation to this could be that more air was introduced when mixing the resin for the 600mbar panel. Both the 900mbar and Autoclave panel have negligible values compared to the others.

Table 18: Summary table of results showing the percentage are of voids based on ImageJ analysis.

Summary

File Edit Font

Slice	Count	Total Area	Average Size	%Area
HL_BLACK.jpg	28	51588	1842.429	1.050
300_BLACK.jpg	173	178508	1031.838	3.632
600_BLACK.jpg	64	228020	3562.812	4.639
900_BLACK.jpg	2	2261	1130.500	0.046
AC_BLACK.jpg	0	0	NaN	0.000

There are multiple reasons this method will be inaccurate, primarily being the manual highlighting of voids. Small voids may not appear visible with there also being a limit to the optical depth of field through the thickness of each sample.

An attempt to quantify the V_v was made using Equation 3, with the recorded values in Table 11. The results yield negative values for Vv, showing there is low reliability in the data as there cannot be a negative V_v. There are several possible causes for this error in values.

The CRAG method used, based on the displacement method, does not account for voids, with values of V_v>1% yielding flawed results. Another lies with not having accurate values for the density of the glass or the cured resin used, as mentioned in Section 2.4.

Therefore, an assumed density of 2550kg/m^3 for E-Glass and 1190kg/m^3 for the cured resin (based on a polyester with similar characteristics) was used in the calculations. Depending on the source of reference, the E-Glass density can increase to 2600 kg/m^3 (Azom.com, 2016). Referencing the work of Lenoe (1970) and Olster (1972), an error of as little as 0.1% in any of the measured parameters can lead to a void content error of 2.5% overall. Using this higher density value, the results increase by ~1%, however still include negative results within the set.

Table 19: Corrected void volume fraction values.

		Experiment				
Property	**Unit**	**HL**	**300**	**600**	**900**	**AC**
Fibre content	**%**	40.77	45.71	47.03	49.33	49.60
Calculated Vv	%	-1.73	-0.18	-0.97	-1.16	-1.15
Corrected Vv	**%**	**1.05**	**2.6**	**1.81**	**1.62**	**1.63**

Application of a correction factor of +2.78 to the values in Table 11, for a fibre density of 2550 kg/m^3, yields a matching value of V_v in the calculations to that recorded for the base-line hand-laminated panel using the planar image analysis (Table 18). The resultant V_v values all become positive (Table 19). Analysis of the corrected values suggests a decrease in void content of ≈1% in the RI panels for a ≈4% increase in V_f however it is unlikely to be a true representation due to the manner in which the results were determined.

5.6. Modulus

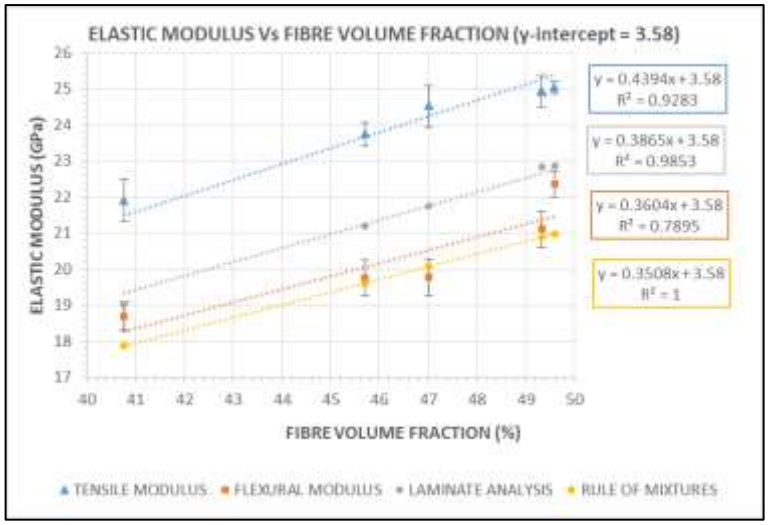

Figure 9: Comparison of experimental, theoretical and simulated modulus against V_f with no (y)-intercept

Figures 9 and 10 represent the elastic modulus for each panel. The tensile and flexural data sets were determined through mechanical testing with the remaining two determined using the calculated V_f of each panel.

The trend lines in Figure 9 are plotted with no set y-intercept, whereas those in Figure 10 were adjusted to intercept at y=3.58, a value that simulates a 0% V_f but accounts for the property of the resin that would remain in the panel.

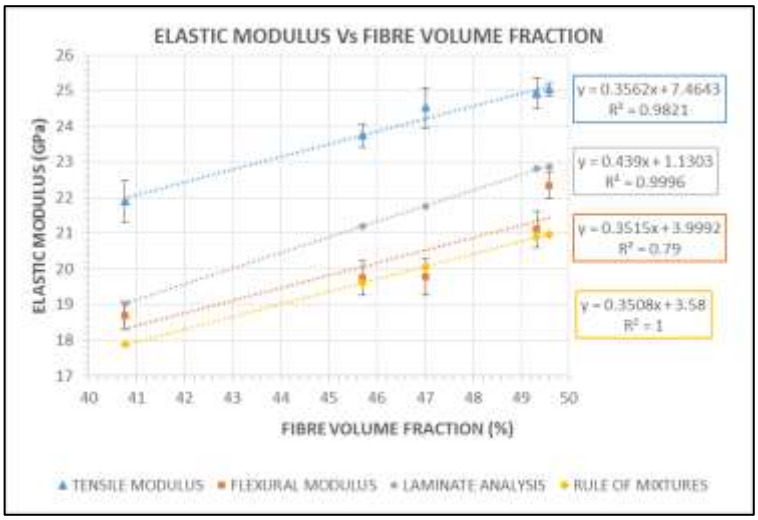

Figure 10: Comparison of experimental, theoretical and simulated modulus against V_f with the (y)-intercept set to the matrix modulus value (3.58 GPa)

The average deviation between the highest recorded values (tensile) and the lowest (RoM) is 3.8GPa or 17.44%. Each method inherently has its own associated issues (Table 16) which may contribute towards this variation in result.

Each dataset shows a positive linear trend-line, signifying that as the relative volume of resin decreases, the modulus value increases. The lowest recorded CoD value is seen for the flexural modulus in Figure 9, with a value of 0.7895. Closer examination of the individual data points shows a lower statistical correlation between test panels for this measurement than the other methods.

The tensile, laminate analysis and RoM have CoD values of 0.9283, 0.9853 & 1 respectively, signifying there is a strong relationship between the data points across the panels as well as the test methods. This conclusion is further backed by the similarity in the gradient of each trend-line, varying by 0.0886 from 0.3508 (RoM) to 0.4394 (tensile).

A reduction in resin content from 59 % in the HL panel to 50% in the AC panel, equates to a real term resin decrease of 15% overall. Based on the values determined using RoM, as they have the highest CoD, there is a 20% increase in modulus of over this drop in resin content.

5.7. Flexural Strength

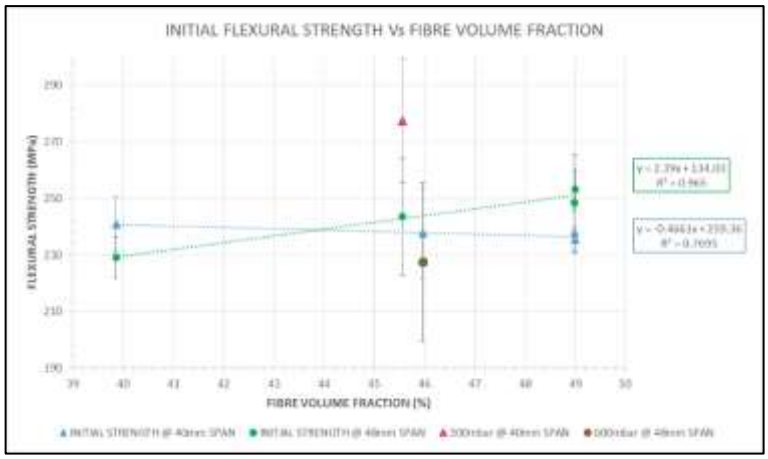

Figure 11: Initial flexural strength against fibre volume fraction for different test spans.

Figure 11 shows the results for the initial flexural strength, defined by the load at which the load/deflection slope no longer obeys Hooke's Law. Experiments were conducted at spans of 40mm and 48mm, with these used due to the range of thicknesses with the hand-laminated specimens exceeding the stipulated 2±0.3mm for a standard Class III specimen, as defined in BS EN ISO 14125:1998+A1:2011.

The results appear inconclusive regarding a specific trend, with a large statistical variation recorded for the majority of specimens. The 48mm span shows an increase in strength with V_f, with the 40mm span showing a decrease. It should also be noted that two data points were deemed anomalies, one outlier from each test span, due to their variance from the other values for the dataset.

The first (300mbar @40mm span) recorded a value of 277.4MPa, 36.5MPa higher than the nearest recorded value. The second (600mbar @48mm span) recorded a value 16.1MPa lower than the closest value.

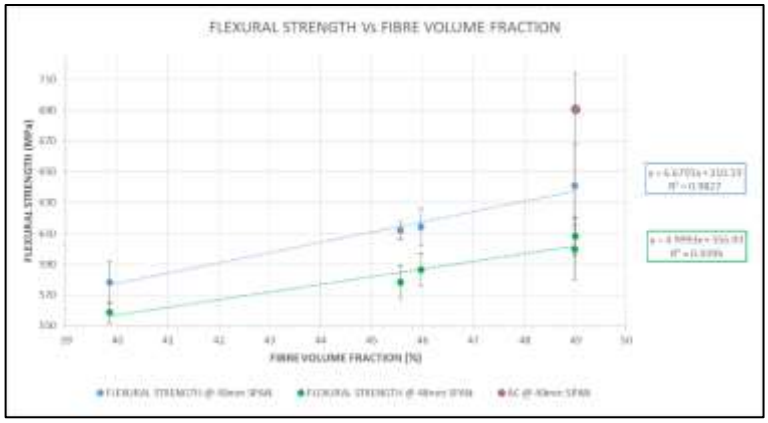

Figure 12: Flexural strength against fibre volume fraction for different test spans.

Figure 12 shows at both spans there is a strong linear relationship between the data, with R^2 values of 0.9827(40mm span) and 0.9395(48mm span). The error bars also show there is little variation between the values recorded for each test panel. Based on the results, for each 1% increase in V_f there is an increase in strength of 6.679MPa.

Judd & Wright (1978) suggest a decrease in flexural strength of 30% for each 1% increase in voids. However, based on the corrected values in Table 18 for the RI panels, there is only a 5% decrease in strength recorded for the 1% increase in V_v further backing the unreliability of the results.

5.8. Apparent Inter-Laminar Shear Strength

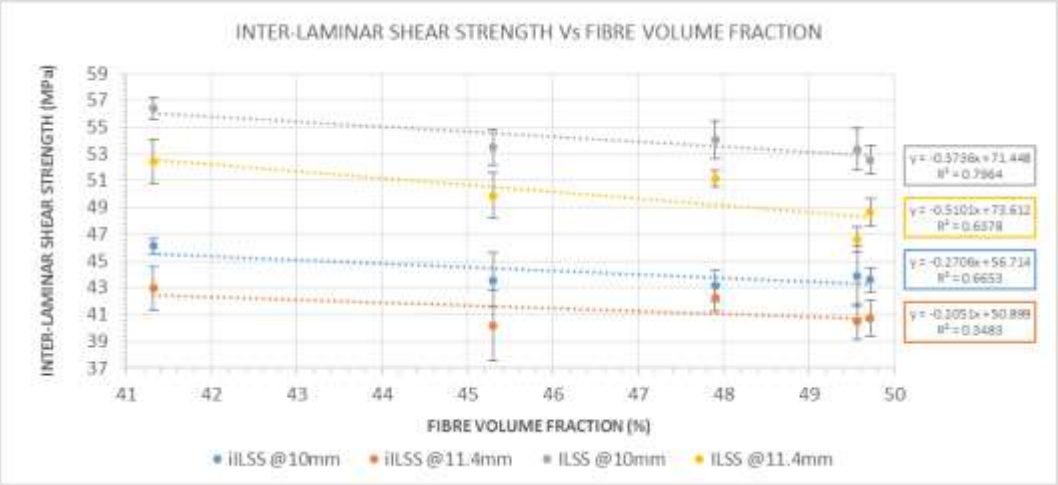

Figure 13: Comparison of initial and inter-laminar shear strengths for different test spans.

ILSS is a matrix/interface dominated property and is a function of thickness rather than fibre content. An ILSS test is typically conducted as a measure of comparison in performance, rather than to provide accurate design properties for the material tested (Adams, 2013).

Two test spans were used to determine the apparent ILSS. The first, 10mm, was based on the span/thickness ratio of 5*h±03 mm as set out in BS EN ISO 14130:1998 for a plate of 2mm thickness. The second span of 11.4mm was 5x the mean thickness of the hand-laminated panel specimens.

Two spans were used to eliminate the possible influence on the results of the extra thickness in the hand-laminated panel (lowest V_f) compared to those manufactured using RI, with the results suggesting a similar drop in strength for all specimens across both spans.

Observation of the error bars in Figure 13 shows that across all specimens there was a significant variation in results for both change in V_f and span. Based on the R^2 value no data set is an exact match to the plotted linear trend-line, with both data-sets recording a decrease in strength as V_f

increases. The results however are consistent with those expected for a well-bonded fibre-matrix interface.

The work of Judd and Wright (1978) suggests for each 1% decrease in voids there should be an increase in strength of 7% however the results of these experiments contradict this. In terms of void content, based on V_v from Table 18 and strength values from Table 14 there is a 1.87% decrease in strength for a 1% decrease in voids. In terms of V_f, for each 1% increase there is a reduction in strength of 0.67% @ 10mm and 0.97% @ 11.4mm.

5.9. Tensile properties

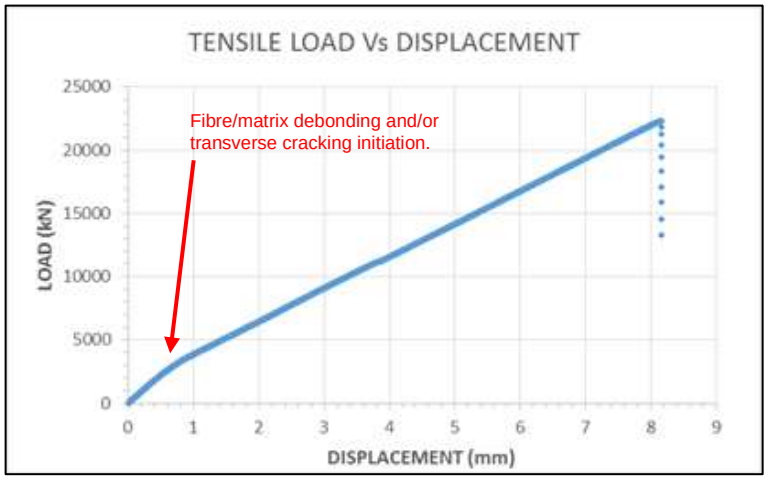

Figure 14: Determining FMD/transverse cracking initiation

With an average value of 0.241%, the value for strain at which possible fibre-matrix-debonding (FMD) and/or transverse cracking (TC) initiate is slightly less than the value of ≈0.3% suggested by Hull and Clyne (1996) for a cross-ply laminate in uniaxial tension.

The values for both load and strain rate are taken at the point where the graph is no longer linear (Figure 14). The value quoted by Hull & Clyne is an approximation, however the deviation in the experimental results could be explained by factors such as the sizing used on the glass preventing a perfect bond at the fibre/matrix interface.

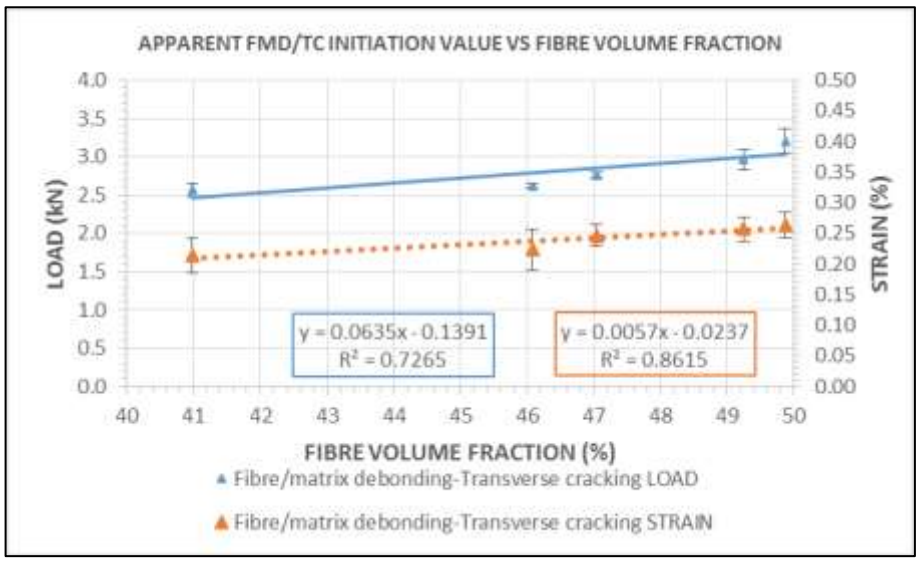

Figure 15: Increase in strain and load for FMD/TC initiation for each panel.

For both the strain and load recorded, there is a progressive increase as V_f increases with a strong correlation between the data and the linear trend-line (Figure 15). This progressive increase could be explained by the reduction in residual resin, reducing the space within which voids can remain leading to a better interfacial bond. A theory backed by the work of Zhu et al. (2008) who saw that voids can affect this bonding between the fibre and matrix and be an initiation site from which transverse cracking occurs.

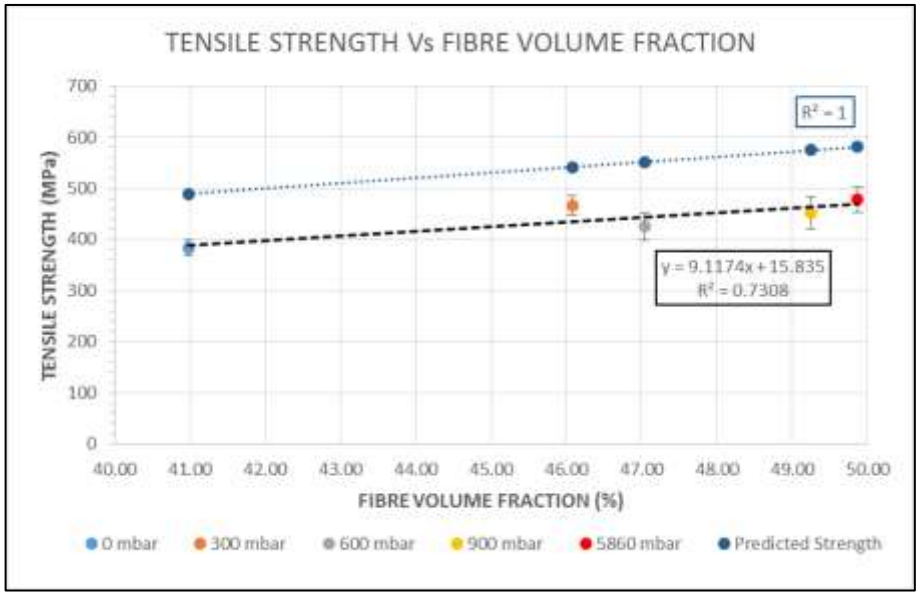

Figure 16: Graph of both experimental and predicted tensile strength Vs fibre volume fraction.

Figure 16 shows the experimental and predicted tensile strengths based on the results from Table 15. It is clear there is a good statistical correlation between the recorded values and the trend-line. The only set of results that

fail to correlate to the trend-line are those recorded for the 300mbar test panel, with a slightly higher value than would be predicted.

Tensile strength is a more fibre dominated mechanical property than the resin dominated ILSS. Although cracking is known to start within the resin at void locations, the final strength is more reliant on the fibres themselves.

The difference seen between the experimental results and the theoretical Kelly-Tyson strength model (1965) could lie with a number of factors. This equation is based on a number of underlying assumptions such as:

- The composite is made up of UD fibres which are perfectly aligned with the load.
- All fibres have identical strength.
- Both fibre and matrix fail at the same percentage strain.
- There is a perfect interface between matrix and fibre.

The tensile strength of a 'virgin' glass fibre, used to represent the fibre strength in the equation, varies depending on reference location. It is unlikely to adequately represent that of the glass in use within the experiment, due to possible issues with damage, alignment and crimp seen in the woven fabric. It is also unlikely all of the assumptions in the equation will be true in the experimental specimens tested, leading to the difference seen between the measured results and those predicted.

Taking into account all of these causes of variation, the experimental results are all within ≈20% of the predicted value. This is also in spite of the presence of the transverse fibres in the composite being omitted from the calculations as noted in the caption to Equation 2.

Comparing the minimum and maximum V_f recorded, for a real term decrease in resin content of ≈14% there is an increase in tensile strength of 94.4MPa, equating to an increase of ≈25% or an increase in strength of 9.1MPa for each 1% increase in V_f.

6. Conclusions

Based on the methodology used and the limitations/flaws identified throughout it can be concluded that:

- With a reduction in resin content and proven reduction in the size of RRV there is a strong positive linear correlation for Elastic modulus, Flexural and Tensile strengths. The ILSS results show a negative relationship between strength and V_f.
- For each 1% increase in V_f there is an increase in property as follows:
    - Elastic modulus (Tensile): 356.2MPa
    - Elastic modulus (Flexural): 351.5MPa
    - Flexural strength: 6.68MPa.
    - Tensile strength: 9.11MPa.

- The ILSS specimens show a decrease in strength of 0.374MPa for each 1% increase in V_f, with the strength value showing a decrease against an assumed decrease in $V_{v,}$ contradicting the work of Judd and Wright (1978).

7. Recommendations

- Further research to determine the constituent material densities would allow more accurate determination of void content based on the calculations used.
- Equivalent experiments using different constituent materials/manufacturing methods would allow comparison of whether there is the same relationship between V_f and mechanical property.
- Refinement of the combination of RI panels and the AC.
- Development of a polishing technique to enhance fibre/matrix contrast.

References

Adams, D. (2013). *The Short Beam Shear Test Method for Composite Materials.* [online] Compositesworld.com. Available at: http://www.compositesworld.com/articles/the-short-beam-shear-test-method-for-composite-materials [Accessed 26 Apr. 2016].

Aono, Y., Hirota, K., Lee, S-H., Kuroiwa, T. and Takita, K. (2008). *Fatigue damage of GFRP laminates consisting of stitched unit layers*. International Journal of Fatigue, Volume 30, Issues 10–11, October–November 2008, pp. 1720-1728.

Åström, B. (1997). *Manufacturing of polymer composites*. London: Chapman & Hall.

Azom.com. (2016). *Properties: E-Glass Fibre*. [online] Available at: http://www.azom.com/properties.aspx?ArticleID=764 [Accessed 20 Apr. 2016].

Basford, D.M., Griffin, P.R., Grove, S.M. and Summerscales, J. (1995). *Relationship between mechanical performance and microstructure in composites fabricated with flow-enhancing fabrics*. Composites, Volume 26, Issue 9, September 1995, pp. 675-679.

Campbell, F. (2010). *Structural composite materials*. Materials Park, Ohio: ASM International.

Daniel, I. and Ishai, O. (2006). *Engineering mechanics of composite materials*. New York: Oxford University Press.

Dong, C. (2011). *Model development for the formation of resin-rich zones in composites processing*. Composites: Part A 42 (2011) pp. 419–424.

Ghiorse, S.R. (1993). *Effect of void content on the mechanical properties of carbon/epoxy laminates*. SAMPE Quarterly, January 1993, 24(2), pp. 54-59.

Guild, F. J. and Summerscales, J. (1993). *Microstructural image analysis applied to fibre composite materials: a review*. Composites, Volume 24, Issue 5, July 1993, pp. 383–393.

Hull, D. and Clyne, T.W. (1996) *An Introduction to Composite Materials* - 2nd edition, Cambridge UP.

Judd, N. C. W. and Wright, W. W. (1978). *Voids and their effects on the mechanical properties of composites - an appraisal*. SAMPE Journal, January/February 1978, 14(1), pp. 10-14.

Kelly, A. and Tyson, W.R. (1965) *Tensile properties of fibre-reinforced metals: copper/tungsten and copper/molybdenum.* Journal of the Mechanics and Physics of Solids, 1965, 13, pp. 329-350.

Kuriyama, T., Mizoguchi, M. and Ogawa, T. (2004). *Effect of injection speed on internal structure and mechanical properties in short glass fibre reinforced polyamide injection mouldings.* Polymers & Polymer Composites, Volume 12, No. 5, 2004, pp. 423-431.

Lenoe, E. M. (1970) *The Effects of Voids on the Mechanical Properties of High Modulus Graphite Fibre/Epoxy Reinforced Composites.* AVSD-0170-70-RR, Avco Corp. Systems Division, Lowell, Massachusetts.

Liu, L., Zhang, B-M., Wang, D-F. and Wu, Z-J. (2006). *Effects of cure cycles on void content and mechanical properties of composite laminates*. Composite Structures, Volume 73, Issue 3, June 2006, pp. 303-309.

Mouritz, A.P. (2007). *Review of z-pinned composite laminates*. Composites Part A: Applied Science and Manufacturing, Volume 38, Issue 12, December 2007, pp. 2383-2397.

Mraz, S. (2014). *Basics of Aerospace Materials: Aluminum and Composites*. [online] Machinedesign.com. Available at: http://machinedesign.com/materials/basics-aerospace-materials-aluminum-and-composites [Accessed 22 Nov. 2015].

Olster, E. F. (1972) *Effects of Voids on Graphite Fibre Reinforced Epoxy Composites.* Final Report, Contract N00019-71-C-0305, U.S Naval Air Systems Command, Washington.

Pearce, N.R.L., Summerscales, J. and Guild, F.J. (2000). *Improving the resin transfer moulding process for fabric-reinforced composites by modification of the fabric architecture*. Composites Part A: Applied Science and Manufacturing, Volume 31, Issue 12, December 2000, pp. 1433-1441.

Pickard, R. (no date). *Manufacturing | Autoclave Design | NetComposites Now*. [online] Netcomposites.com. Available at: http://www.netcomposites.com/guide-tools/guide/manufacturing/autoclave-design/ [Accessed 24 Nov. 2015].

Quinn, J. A. and Randall, J.E. (1990). *Compliance of composite reinforcement materials*. Proceedings of the Fourth International Conference on Fibre Reinforced Composites, Liverpool, 27-29 March 1990, paper C400/046. Proceedings of the Institution of Mechanical Engineers 1990-3, pp. 105-112.

Robitaille, F. and Gauvin, R. (2004). *Compaction of textile reinforcements for composites manufacturing. I: Review of experimental results*. Polymer Composites, 1198 19(2), pp. 198-216.

Stickler, P.B. and Ramulu, M. (2001). *Investigation of mechanical behaviour of transverse stitched T-joints with PR520 resin in flexure and tension*. Composite Structures, Volume 52, Issues 3–4, May–June 2001, pp. 307-314.

Stone, D.E.W. and Clarke, B. (1975). *Ultrasonic attenuation as a measure of void content in carbon-fibre reinforced plastics*. Non-Destructive Testing, Volume 8, Issue 3, 1975, pp. 137-145.

Summerscales, J. (no date.A). MATS347 Composites Design and Manufacture. [online] Fose1.plymouth.ac.uk. Available at: https://www.fose1.plymouth.ac.uk/sme/MATS347/MATS347A3%20IfaceMeso.htm#voids [Accessed 4 May 2016].

Summerscales, J. (1987). *Non-destructive testing of fibre-reinforced plastics composites – Vol. 1*. London: Elsevier Applied Science.

Summerscales, J. (1990a). *Non-destructive testing of advanced composites: a review of recent advances*. British Journal of Non-Destructive Testing, November 1990, 32(11), pp. 568-577.

Summerscales, J. (1990b). *Non-destructive testing of fibre-reinforced plastics composites – Vol. 2*. London: Elsevier.

Summerscales, J. (1998). *Microstructural characterisation of fibre-reinforced composites*. Boca Raton, FL: CRC Press.

Tan, K.T., Yoshimura, A., Watanabe, N., Iwahori, Y. and Ishikawa, T. (2013) *Effect of stitch density and stitch thread thickness on damage progression and failure characteristics of stitched composites under out-of-plane loading*. Composites Science and Technology, Volume 74, 24 January 2013, pp. 194-204.

Toll, S. (1998). *Packing Mechanics of Fibre Reinforcements*. Polymer engineering and science, Volume 38, no. 8, August 1998, pp. 1337-1350.

Toll, S. and Månson, J-A.E., (1994) *An analysis of the compressibility of fibre assemblies*. Proceedings of the Sixth International Conference on Fibre Reinforced Composites, Newcastle-upon-Tyne, 29-31 March 1994, paper 25. Institute of Materials Conference Papers series, pp. 25/1-25/10.

Valenza, A. and Fiore, V. (2010). *Influence of resin viscosity and vacuum level on mechanical performance of sandwich structures manufactured by vacuum bagging*. Advanced Polymer Technology, 29: pp. 20–30.

Virk, A.S., Hall, W. and Summerscales, J. (2012) *Modulus and strength prediction for natural fibre composites*. Materials Science and Technology, 2012, 28(7), pp. 864-871.

Williams, C.D., Grove, S.M. and Summerscales, J. (1998). *The compression response of fibre-reinforced plastic plates during manufacture by the resin infusion under flexible tooling method*. Composites Part A: Applied Science and Manufacturing, Volume 29, Issues 1–2, 1998, pp. 111-114.

Witik, R.A., Gaille, F., Teuscher, R., Ringwald, H., Michaud, V. and Månson, J.A.E. (2012). *Economic and environmental assessment of alternative production methods for composite aircraft components*. Journal of Cleaner Production, Volumes 29–30, July 2012, pp. 91-102.

Zhu, H., Wu, B., Li, D., Zhang, D. and Chen, Y. (2011). *Influence of Voids on the Tensile Performance of Carbon/epoxy Fabric Laminates*. Journal of Materials Science & Technology, Volume 27, Issue 1, January 2011, pp. 69-73.